Robust detection of deeply subwavelength pits in simulated optical data-storage disks using photonic jets

Soon-Cheol Kong,[1,a)] Alan V. Sahakian,[1,2] Alexander Heifetz,[2] Allen Taflove,[1] and Vadim Backman[2]
[1]*Department of Electrical Engineering and Computer Science, Northwestern University, Evanston, Illinois 60208, USA*
[2]*Department of Biomedical Engineering, Northwestern University, Evanston, Illinois 60208, USA*

(Received 22 January 2008; accepted 5 March 2008; published online 28 May 2008)

We report a means to detect deeply subwavelength pits in optical data-storage media by employing the recently observed giant backscattering perturbation phenomenon of the photonic jet. We conducted microwave experiments with dimensionally scaled-up pits and lands in a simulated optical data-storage device. These measurements were backed up by three-dimensional finite-difference time-domain computational solutions of Maxwell's equations. Results indicate that pits having a lateral area of 0.025 square wavelengths, i.e., much smaller than current BluRay™ device features, can be robustly detected with a contrast ratio approximately 28 dB greater than that provided by a lens system. © *2008 American Institute of Physics*. [DOI: 10.1063/1.2936993]

Since 2004, a substantial literature has developed regarding the existence, properties, and potential applications of the *photonic jet* (or *nanojet*, when observed at optical wavelengths).[1–12] The photonic jet is a narrow, high-intensity beam that propagates into the background medium from the shadow-side surface of a plane-wave illuminated lossless dielectric cylinder or sphere of diameter comparable to the wavelength. Some of the properties of the photonic jet are as follows. (1) It is a nonresonant phenomenon, i.e., it can appear for a wide range of the electrical size of the dielectric cylinder or sphere if the refractive index contrast relative to the background medium is less than about 2:1. (2) It has a high intensity of up to about 1000 times that of the illuminating wave. (3) Its full width at half maximum beamwidth is between one-third and one-half wavelength in the background medium and is only weakly dependent upon the size of the dielectric cylinder or sphere.[11] (4) It propagates with little divergence for several wavelengths. (5) The insertion within a photonic jet of a particle as small as 1/100th of the size of the dielectric cylinder or sphere causes a perturbation of the backscattered power of the cylinder or sphere that is comparable to its total backscattered power.[2,5,7]

In this letter, we report the results of our laboratory experiments and three-dimensional (3D) finite-difference time-domain (FDTD) computational electrodynamics simulations[13] which investigated the potential use of the photonic jet to detect deeply subwavelength pits in an optical data-storage disk. Our laboratory experiments were conducted near 30 GHz (free-space wavelength $\lambda_0=10$ mm). Pits and lands of appropriately scaled dimensions were machined in an aluminum plate coated with a low-loss dielectric having an optimized thickness.

Figure 1 shows a dimensionally scaled simulated optical disk used for one of our microwave experiments. The machining of this aluminum plate emulates the pits-on-groove configuration used by BluRay™ disks.

Figure 2 shows the experimental setup for our microwave backscattering measurements. An Agilent 8722ES vector network analyzer (VNA) was used to generate the microwave signal and measure the backscattered response. A WR28-to-WR90 tapered waveguide transition connected to the VNA was employed as a horn antenna in a monostatic configuration. Microwave absorbers were used to reduce spurious reflections and the antenna was oriented to radiate vertically upward. The target of this illumination was a 50.8 mm ($5.1\lambda_0$) diameter acrylic sphere (refractive index $n=1.60$) mounted on a Styrofoam support 400 mm ($40\lambda_0$) above the aperture of the antenna in its far field.

The resulting approximate plane-wave illumination of the acrylic sphere caused it to emit a microwave jet from its top surface toward a machined aluminum plate (simulating the optical disk) located above the acrylic sphere. This plate was covered with a layer of RT/Duroid5880, a low-loss dielectric material of refractive index $n=1.48$. (In the optical wavelength range, a protective layer made of polymethyl methacrylate has a same refractive index.) The thickness of the dielectric layer was optimized for the maximum no-pit-to-pit ratio. The simulated optical disk under test was mounted on an *x*-*y*-*z* translator for fine position adjustments.

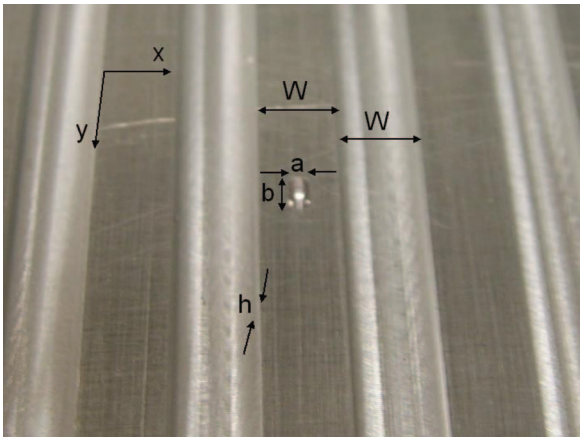

FIG. 1. (Color) Photograph of a sample machined aluminum disk with a pit on groove structures. Dimensions are scaled up to 30 GHz ($\lambda_0=10$ mm): $a=1.25$ mm ($\lambda_0/8$), $b=2$ mm ($\lambda_0/5$), $W=4$ mm ($0.4\lambda_0$), and $h=1$ mm ($\lambda_0/10$).

a)Electronic mail: sch.kong@gmail.com.

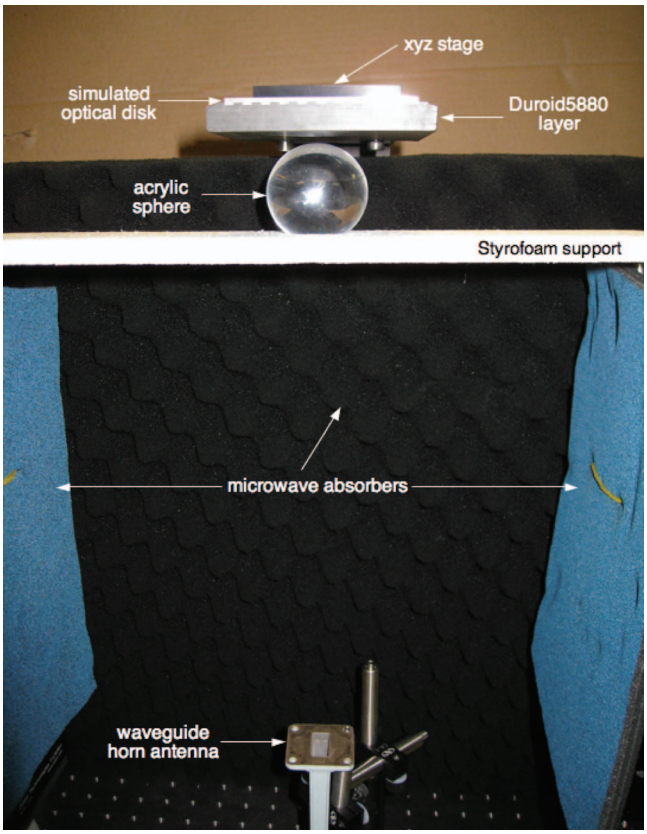

FIG. 2. (Color) Photograph of the experimental measurement setup.

A laser beam was used to adjust the boresight of the horn antenna to pass vertically through the center of the acrylic sphere along the line perpendicular to the machined aluminum plate above the sphere. Once adjusted, the boresight of the antenna, and hence the boresight of the microwave jet, could repeatably target specific pit or no-pit locations on the aluminum plate for measurement of perturbations of the composite backscattered microwave signal.

Data for the backscattered microwave power versus frequency were obtained by measuring S_{11} with the VNA. For purposes of calibration, an S_{11} dataset was first obtained and digitally stored for the system consisting only of the VNA, the connecting cable, the horn antenna, the microwave absorbers, and the Styrofoam support of the acrylic sphere. Digitally subtracting this dataset repeatedly over a period of time comparable to that needed for the experimental procedure indicated an effective noise floor of −80 dBm. After placing the acrylic sphere upon its Styrofoam support, the measured S_{11} increased by approximately 25–30 dB, corresponding to the backscattering by this sphere alone. Then, placing the RT/Duroid5880-coated aluminum disk above the acrylic sphere increased the measured S_{11} by up to an additional 30 dB for the no-pit case (i.e., the microwave jet impinging upon a simulated land in the aluminum disk).

The complete calibration and measurement procedures were repeated multiple times over a period of several days to establish experimental uncertainty bounds. We determined that the maximum no-pit-to-pit ratio derived from the measured S_{11} data had an uncertainty of approximately ± 2 dB, and the frequency at which the maximum no-pit-to-pit ratio occurred had an uncertainty of approximately $\pm 1\%$.

Computational support for our laboratory experiments was provided by conducting high-resolution, 3D, pure scattered-field FDTD simulations.[13] Each FDTD model employed a uniform Cartesian grid of 0.25 mm ($\lambda_0/40$) spatial resolution with perfectly matched layer absorbing outer grid boundaries. The aluminum plate was treated as a perfect electric conductor, which is appropriate at microwave frequencies. Near-field and far-field sinusoidal (phasor) data were obtained via discrete Fourier transformation of the transient response generated by a modulated Gaussian plane-wave source. We note that the FDTD models differed from the laboratory experiments primarily in assuming a perfect plane-wave illumination of the acrylic sphere, whereas the illumination actually provided by the horn antenna exhibited some amount of amplitude and phase nonuniformity at the location of the acrylic sphere due to its finite distance from the horn (albeit in its far field).

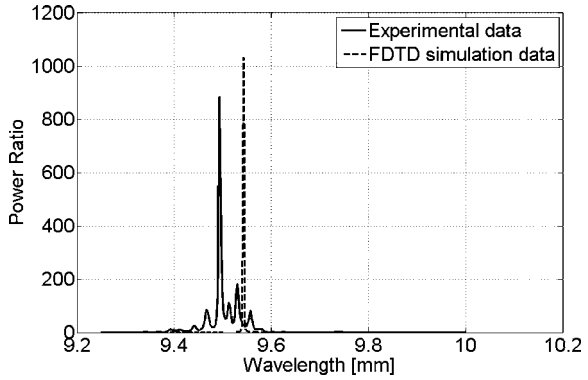

FIG. 3. Comparative experimental and FDTD data for the no-pit-to-pit power ratio vs wavelength for a rectangular pit of lateral dimensions 1.25 mm ($\lambda_0/8$) in the x direction $\times 2$ mm ($\lambda_0/5$) in the y direction. The pit depth was 2 mm ($\lambda_0/5$) in the z direction. The thickness of the RT/Duroid5880 layer covering the aluminum disk was 11.75 mm ($1.175\lambda_0$), and the distance between the acrylic sphere and the Duroid layer was 4 mm ($0.4\lambda_0$). Both datasets show a peak no-pit-to-pit power ratio that is approximately 700 times (i.e., 28 dB) greater than the 1.2 value reported in Ref. 14 using a conventional lens for an octagonal pit of approximately the same lateral area in square wavelengths.

Figure 3 illustrates an example of our comparative experimental and FDTD data for the no-pit-to-pit power ratio versus wavelength for a rectangular pit of lateral dimensions 1.25 mm ($\lambda_0/8$) in the x direction $\times 2$ mm ($\lambda_0/5$) in the y direction. The pit depth was 2 mm ($\lambda_0/5$) in the z direction. The thickness of the RT/Duroid5880 layer covering the aluminum disk was 11.75 mm ($1.175\lambda_0$), and the distance between the acrylic sphere and the Duroid layer was 4 mm ($0.4\lambda_0$). The measurements and the FDTD model agree within 1 dB in amplitude and within 1% in wavelength. Both the measured data and the FDTD computations show a peak no-pit-to-pit power ratio that is approximately 700 times (i.e., 28 dB) greater than the 1.2 value reported in Ref. 14 using a conventional lens for an octagonal pit of approximately the same lateral area in square wavelengths. Additional FDTD modeling results (not reported here) have shown that the peak no-pit-to-pit power ratio is also sensitive to the pit depth, and thus, data capacity could conceivably be increased by employing pit-depth modulation.[15]

Figure 4 provides the results of FDTD computations which illustrate the physics underlying the high sensitivity of pit detection shown in Fig. 3. Figures 4(a) and 4(b) visualize the scattering of the microwave jet by the Duroid-coated aluminum plate for the no-pit and pit cases of Fig. 3, respectively. Figures 4(a) and 4(b) both show strong backscattering

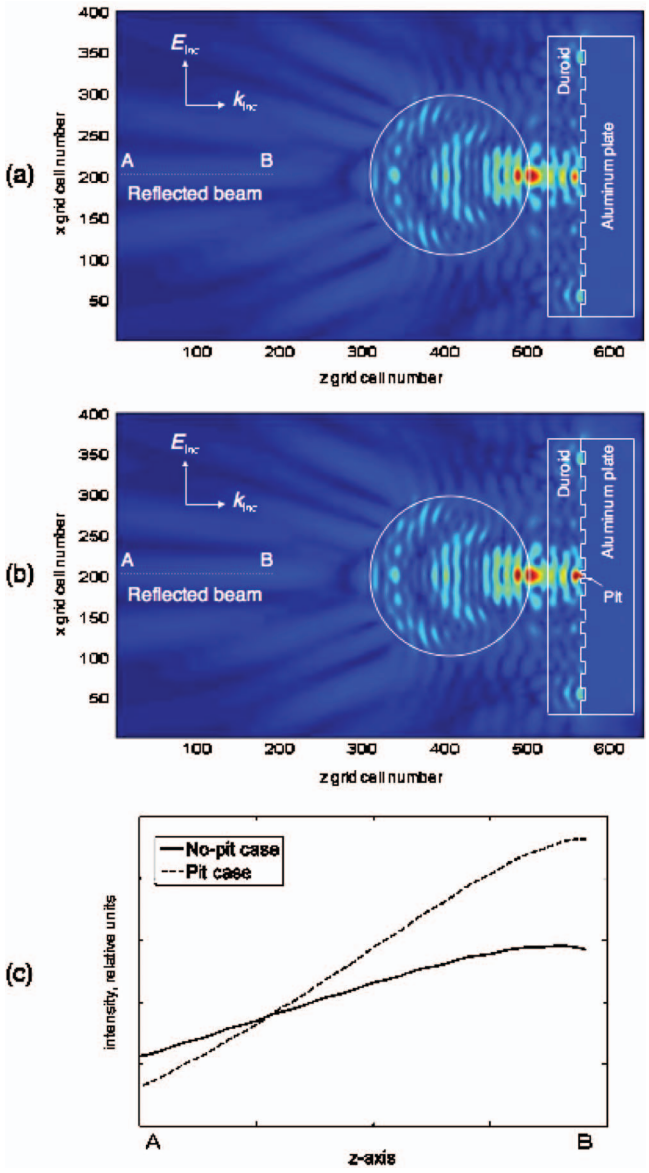

FIG. 4. (Color) FDTD-computed microwave intensity distributions relevant to Fig. 3. (a) Interaction of the photonic jet with the Duroid-coated aluminum plate for the no-pit case. The maximum intensity is ~90 times the incident. (b) Same as (a) but with a 1.25 mm $(\lambda_0/8)\times 2$ mm $(\lambda_0/5)$ $\times 2$ mm deep $(\lambda_0/5)$ pit in the aluminum plate present in the jet. There is now a strong intensity localization in the vicinity of the pit with a peak value of ~225 times the incident. (c) The backscattered intensity decreases with propagation distance faster for the pit case of (b) than for the no-pit case of (a).

in the $-z$ direction. However, for the pit case of Fig. 4(b), we see a strong localization of the intensity in the vicinity of the pit with a peak value of ~225 times the incident, and a faster decay of the backscattered wave with propagation distance than for the no-pit case of Fig. 4(a). This faster decay is illustrated in Fig. 4(c), which graphs the microwave intensity along line *AB* shown in Figs. 4(a) and 4(b). This faster decay in the near field yields a much smaller far-field backscattering, which is what is observed experimentally as well as computationally.

In summary, we employed the recently observed giant backscattering perturbation phenomenon of the photonic jet to go beyond the Abbe diffraction limit in detecting deeply subwavelength pits in a simulated optical data-storage medium. Laboratory experiments with dimensionally scaled-up pits and lands were carried out at a microwave wavelength. These measurements were backed up by 3D FDTD computational modeling. Results indicate that deeply subwavelength pits having a lateral area of 0.025 square wavelengths, i.e., much smaller than current BluRay™ device features, can be robustly detected with a contrast ratio approximately 28 dB greater than that provided by a lens system.

While the solid immersion lens could provide an optical resolution comparable to that of the photonic nanojet, the ray-based solid immersion lens does not possess the nanojet's "unique combination of features in the angular spectrum:…finite content of propagating spatial frequencies, a small but finite content of evanescent spatial frequencies, and, most importantly, a peculiar distribution of the phase."[3] These features apparently underlie the nanojet's giant backscattering perturbation phenomenon that is the driver behind the robust pit detection reported herein.

Regarding several specifics of implementing nanojet technology at optical wavelengths, (a) a low-index aerogel could be used to mount the dielectric microsphere without impacting the characteristics of the nanojet. (b) In our ongoing computational modeling work (not reported here), we have determined that after compensating adjustments of the pit depth and dielectric coating thickness, the plasmonic characteristic of the metal at optical wavelengths would cause little change in the robustness of the pit detection. (c) The optical illumination of the microsphere would be much closer to the ideal plane wave assumed in our FDTD model than achieved in our microwave experiments. Hence, the illumination wavelength required for optimum pit detection could be engineered with sufficient accuracy to accommodate the narrow optical linewidth of the pit-detection technique.

We conclude that using photonic nanojets to read optical data-storage device pits would allow detection of pits that are considerably smaller than the present state of the art, while involving only available materials and allowing manufacturable separations between the surface of the storage medium and the optical read head.

This work was supported in part by National Science Foundation Grant No. BES-0522639.

[1]Z. Chen, A. Taflove, and V. Backman, Opt. Express **12**, 1214 (2004).
[2]X. Li, Z. Chen, A. Taflove, and V. Backman, Opt. Express **13**, 526 (2005).
[3]A. V. Itagi and W. A. Challener, J. Opt. Soc. Am. A **22**, 2847 (2005).
[4]S. Lecler, Y. Takakura, and P. Meyrueis, Opt. Lett. **30**, 2641 (2005).
[5]Z. Chen, X. Li, A. Taflove, and V. Backman, Opt. Lett. **31**, 196 (2006).
[6]Z. Chen, A. Taflove, and V. Backman, Opt. Lett. **31**, 389 (2006).
[7]A. Heifetz, K. Huang, A. V. Sahakian, X. Li, A. Taflove, and V. Backman, Appl. Phys. Lett. **89**, 221118 (2006).
[8]A. M. Kapitonov and V. N. Astratov, Opt. Lett. **32**, 409 (2007).
[9]S. Lecler, S. Haacke, N. Lecong, O. Crégut, J.-L. Rehspringer, and C. Hirlimann, Opt. Express **15**, 4935 (2007).
[10]K. J. Yi, H. Wang, Y. F. Lu, and Z. Y. Yang, J. Appl. Phys. **101**, 063528 (2007).
[11]A. Heifetz, J. J. Simpson, S.-C. Kong, A. Taflove, and V. Backman, Opt. Express **15**, 17334 (2007).
[12]M. Gerlach, Y. P. Rakovich, and J. F. Donegan, Opt. Express **15**, 17343 (2007).
[13]A. Taflove and S. C. Hagness, *Computational Electrodynamics: The Finite-Difference Time-Domain Method*, 3rd ed. (Artech House, Boston, 2005).
[14]J. A. C. Veerman, A. J. H. Wachters, A. M. van der Lee, and H. P. Urbach, Opt. Express **15**, 2075 (2007).
[15]http://statusreports.atp.nist.gov/reports/94-01-0115.htm